Technical Innovations & Patient Support in Radiation Oncology 14 (2020) 21–29

Contents lists available at ScienceDirect

Technical Innovations & Patient Support in Radiation Oncology

journal homepage: www.elsevier.com/locate/tipsro

Research article

Analysis of dose using CBCT and synthetic CT during head and neck radiotherapy: A single centre feasibility study

Lisa K Hay [a,*], Claire Paterson [a,1], Philip McLoone [b], Eliane Miguel-Chumacero [c], Ronan Valentine [c], Suzanne Currie [c], Derek Grose [a], Stefano Schipani [a], Christina Wilson [a], Ioanna Nixon [a], Allan James [a], Aileen Duffton [a,1]

[a] Department of Clinical Oncology, Beatson West of Scotland Cancer Centre, Glasgow 1053 Great Western Road, Glasgow G12 0YN, United Kingdom
[b] Institute of Health & Wellbeing, University of Glasgow, University Ave, Glasgow G12 8QQ, United Kingdom
[c] Department of Radiotherapy Physics, Beatson West of Scotland Cancer Centre, 1053 Great Western Road, Glasgow G12 0YN, United Kingdom

ARTICLE INFO

Article history:
Received 22 November 2019
Received in revised form 31 January 2020
Accepted 25 February 2020

Keywords:
Head and neck cancer
Cone-beam CT
Dose
Radiotherapy
Synthetic CT
Deformable

ABSTRACT

Objectives: The study aimed to assess the suitability of deformable image registration (DIR) software to generate synthetic CT (sCT) scans for dose verification during radiotherapy to the head and neck. Planning and synthetic CT dose volume histograms were compared to evaluate dosimetric changes during the treatment course.

Methods: Eligible patients had locally advanced (stage III, IVa and IVb) oropharyngeal cancer treated with primary radiotherapy. Weekly CBCT images were acquired post treatment at fractions 1, 6, 11, 16, 21 and 26 over a 30 fraction treatment course. Each CBCT was deformed with the planning CT to generate a sCT which was used to calculate the dose at that point in the treatment. A repeat planning CT2 was acquired at fraction 16 and deformed with the fraction 16 CBCT to compare differences between the calculations mid-treatment.

Results: 20 patients were evaluated generating 138 synthetic CT sets. The single fraction mean dose to PTV_HR between the synthetic and planning CT did not vary, although dose to 95% of PTV_HR was smaller at week 6 compared to planning (difference 2.0%, 95% CI (0.8 to 3.1), p = 0.0). There was no statistically significant difference in PRV_brainstem or PRV_spinal cord maximum dose, although greater variation using the sCT calculations was reported. The mean dose to structures based on the fraction 16 sCT and CT2 scans were similar.

Conclusions: Synthetic CT provides comparable dose calculations to those of a repeat planning CT; however the limitations of DIR must be understood before it is applied within the clinical setting.

Introduction

Radiotherapy (RT) is used as a primary treatment or as an adjunct to surgery in squamous cell cancer (SCC) of the head and neck (H&N) [1–3]. Volumetric arc therapy (VMAT) enables highly conformal RT doses to be delivered to target volumes, whilst achieving acceptable dose constraints to the organs at risk (OAR) [3–5]. However, due to the proximity of OAR to target volumes, H&N radiotherapy planning and treatment delivery remains challenging [5].

During RT treatment anatomical changes caused by tumour response, inflammation and weight loss are commonly reported [1,6]. Discrepancies in patient positioning can affect the delivered dose, causing increases in the dose to the OAR and reducing dose to the tumour [1,3,7,8]. Precise immobilisation and image guided RT (IGRT) is crucial to minimise these effects. IGRT allows set-up errors to be corrected prior to treatment delivery and ensures the planned dose is consistently delivered throughout treatment [8–12].

Abbreviations: CBCT, Cone Beam Computed Tomography; sCT, synthetic Computed Tomography; pCT, planning Computed Tomography; GTV, Gross Tumour Volume; CTV, Clinical Target Volume; PTV, Planning Target Volume; OAR, Organs at Risk; IGRT, Image Guided Radiotherapy; SCC, Squamous Cell Carcinoma; VMAT, volumetric arc therapy; RT, radiotherapy; ART, adaptive radiotherapy; DIR, deformable image registration; DVH, dose volume histogram; TPS, treatment planning system; OPSCC, oropharyngeal squamous cell cancer; PRV, planning organ at risk volume.

* Corresponding author.
E-mail address: Lisa.Hay@ggc.scot.nhs.uk (L.K Hay).
[1] Joint last authors.

https://doi.org/10.1016/j.tipsro.2020.02.004

The modality and scheduling of verification images for IGRT and adaptive radiotherapy (ART) are not standardised across UK departments. Repeat computed tomography (CT) or cone-beam CT (CBCT) are often applied although protocols are dependent on available clinical resources rather than established best practice [4,7,11–13]. No guidelines support optimal time points for dose to be verified during H&N RT, however some studies suggest dosimetric changes occur early in the treatment course [8,14,15]. Equally, factors predicting the need for ART (e.g. patient weight loss, tumour staging etc.) are not well defined [16].

Dose verification in our own centre relies on a repeat planning CT mid-way through treatment. The treatment dose is recalculated on the repeat CT and the dose delivered to critical OAR assessed by the treating oncologist. The process is resource intensive and we have found through clinical audit that the vast majority of patients do not require a change to their treatment plan.

Recent studies have suggested that deformable image registration (DIR) for dose verification during radiotherapy may be useful [1,4]. An example of this is using the CBCTs obtained during the treatment course to deform and register the planning CT (pCT) to the CBCT anatomy. This generates a synthetic CT (sCT) set with the Hounsfield units (HU) of the planning CT. This allows monitoring of the patient's treatment plan at different points during the course introducing greater potential for the implementation of ART.

The aim of this study was to assess the suitability of DIR software to generate synthetic CT scans for dose verification during radiotherapy to the H&N. Differences in dosimetry data obtained from the planning and synthetic CT dose volume histograms (DVHs) were evaluated during the treatment course.

Methods

Patient selection

Eligible patients had locally advanced (stage III, IVa and IVb, UICC/AJCC TNM staging system 7th edition) oropharyngeal squamous cell cancer (OPSCC) and received primary RT or chemoradiotherapy (CRT).

Ethical consideration

Patients were treated and consented as standard of care; therefore no ethical approval was required. This retrospective service evaluation was approved by the Beatson West of Scotland Cancer Centre's management group and NHS Greater Glasgow and Clyde's Research and Development department.

Immobilisation & planning CTs

Patients were positioned supine, immobilised with a custom made 5-point thermoplastic head and shoulder mask (Klarity Medical Products, Newark, Ohio), individual foam headrest and knee support. Planning CTs were obtained using a Phillips Brilliance Big Bore scanner (Philips Medical Systems B.V, The Netherlands); slice thickness 2 mm. Scan extent was from vertex to below carina. Planning CTs were acquired at baseline (pCT1) and at fraction 16 of radiotherapy (pCT2). Intravenous contrast was given to patients for the baseline CT but not at fraction 16.

Target delineation & treatment

Gross tumour volumes (GTV) consisting of the primary tumour and known involved lymph nodes were delineated by the clinical oncologist (CO) [17]. GTVs were grown by 1–2 cm to create high risk clinical target volumes (CTV_HR). A margin of 3–5 mm around the CTVs was applied to generate the high risk planning target volumes (PTV_HR) [18,19]. Low risk nodal areas were outlined to generate low risk clinical and planning target volumes respectively (CTV_LR and PTV_LR). Planning organ at risk volumes (PRV) were generated by applying a 3–5 mm isotropic margin around critical OAR. PTVs were cropped from body surface by 5 mm to account for calculation uncertainties in the planning algorithm.

The prescribed dose was 6500 cGy to PTV_HR and 5400 cGy to PTV_LR in 30 fractions. VMAT plans were created within the Eclipse™ treatment planning system (TPS) (Varian Medical System, Palo Alto, CA) and optimised using the inverse planning Analytical Anisotropic Algorithm (AAA Version 13.6.23). The department protocol for the head and neck VMAT dose constraints was established through the outcomes of the PARSPORT trial [20]. Dose constraints applied were mean dose (Dmean) < 2400 cGy for parotid glands (PG), maximum dose (Dmax) $\leq$ 4800 cGy for PRV_spinal cord, Dmax < 5400 cGy for PRV_brainstem and dose to 95% of the PTV_HR (D95%) $\geq$ 95% of the prescribed dose. Target volume dose coverage and OAR sparing was visually assessed and quantified using DVHs.

Treatment was delivered using 6MV VMAT, 2 full arcs, 600MU/min, on a TrueBeam® linear accelerator. Cisplatin 100 mg/m2, day 1 and 22 was given concurrently with radiotherapy in eligible patients.

Image verification process

Orthogonal KV-images were registered with a digitally reconstructed radiograph (DRR) created from pCT1 and online shifts applied daily prior to treatment delivery. A post-treatment CBCT was acquired at fractions 1, 6, 11, 16, 21 and 26. Due to the limited field of view (FoV) on CBCT compared to pCT1, priority was given to inclusion of the brainstem and where possible also PTV_HR in the overlap region, meaning not all structures were included in their entirety in the CBCTs. Each CBCT was reviewed offline by the clinician who evaluated soft tissue changes, volumetric data and the dose distribution.

Contouring and image registration

An offline rigid image registration between each CBCT and pCT1 was performed in the image registration workspace of Eclipse™. The region of interest (ROI) was manually selected by the therapeutic radiographer (RTT) as mid brainstem to below PTV_HR in the craniocaudal direction, behind spinal vertebrae posteriorly and inclusive of the mandible anteriorly. This ROI was applied to all registrations within the study. The images were rigidly registered using the auto-registration tool to align the bony anatomy. The structure set from pCT1 was then duplicated to each CBCT scan. A visual check of the structures on the CBCT was undertaken to confirm the match. In the contour workspace, the parotid glands were manually amended on each CBCT, by the investigating RTT and checked by the CO. The original structures were applied to all registrations throughout the study, with the exception of the parotid glands. There was insufficient clarity on the CBCT and sCT to make adjustment to other structures.

Deformable synthetic image creation

The DIR software used during the study was Varian Velocity™. The starting point for the DIR process was the rigid online CBCT-pCT match [21]. A b-spline deformation algorithm (3-pass deformable registration for finer detail) was used with a noise filter applied to the CBCT to reduce noise, enhance the image contrast and to improve the DIR process.

The pCT was registered to the anatomy of each weekly CBCT and then reshaped, to create a synthetic CT through DIR. The sCT is a new image set where the volume boundaries are the same as the CBCT within the overlap region. Outside the overlap area the primary voxels were copied without deformation. The deformed reshaped volume (sCT) has the Hounsfield units (HU) of the primary CT1 and the anatomy of the CBCT within the overlap region of both the images involved in the DIR. To validate the generated sCT a rigid registration between the sCT and CBCT was undertaken and visually assessed using the spy glass tool.

DIR quality assurance (QA) process

The DIR depends on the image similarity and acquisition quality. For evaluating our deformable fusions and the resulting sCTs, the Velocity™ QA toolkit was used as follows:

- Deformable vector field and grid analysis: Velocity allows quick display of the direction vectors and/or displacement grid to review the manner and method voxels deformed over the volume. This allows evaluation of cases where voxels may have not displaced in congruence with their regional neighbours, such as voxel jumping, unnatural folding, or extreme volume changes.
- Spy Glass Tool – Allows visual image assessment to verify the alignment of the tissue overlay, to detect unusual characteristics or mismatches, such as holes, gaps, swirling, folding and extreme shrinking or stretching.

The DIR was visually validated by Velocity™ competent physicists and a RTT. The sCT images were assessed by visually analysing their likeness to the CBCT, evaluating the volumes appearance as described above (Fig. 1).

Image registration – CBCT with sCT

After DIR, each sCT was imported and rigidly registered with the CBCT within the TPS. The amended CBCT structure set was then copied to the corresponding sCT. The structures were visually assessed on the sCT for any discrepancies which may have occurred during the deformation process; however no further amendments were made to the structure set.

Plan re-calculation and dose comparison

Fig. 2 outlines the points during treatment when sCT images were created. Verification plans were created for each sCT data set and the dose was re-calculated by applying the pre-set monitor unit values of the original pCT1 plan. The planned cumulative dose during treatment based on pCT1 was compared to the observed cumulative dose based on the weekly sCT plans.

Comparison of the 95% dose distribution to PTV_HR on both the sCT and pCT was visually assessed for similarity, using the dose colour wash. The dose coverage, the dose conformance with the volume, areas outside the volume which were receiving 95% of dose and the position of any hotspots greater than 105% were assessed. The dose distribution on the sCT was acceptable if it showed a likeness to the pCT1 plan used for treatment and the department dose constraints were met, during DVH comparison (Fig. 3).

Mid-point dose verification

At fraction 16 a rigid registration between pCT1 and planning CT2 (pCT2) was performed. The structure set from pCT1 was copied to pCT2, after the bony anatomy was aligned within the ROI. Within the external beam planning workspace the dose was

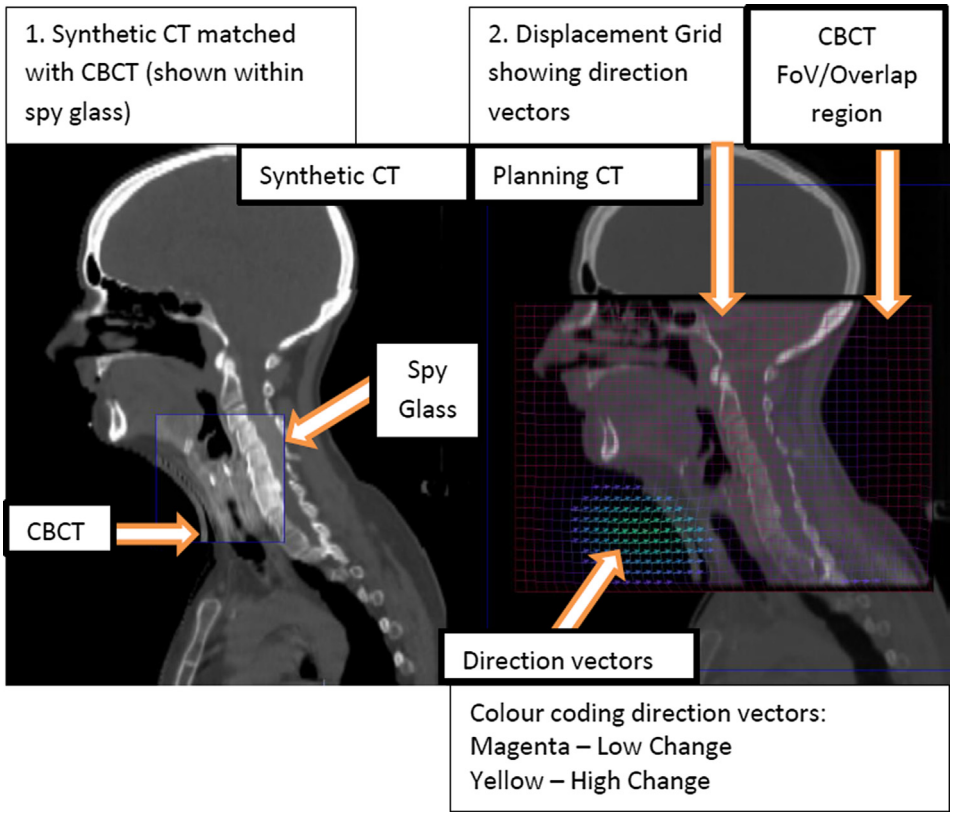

Fig. 1. Deformable image registration QA process.

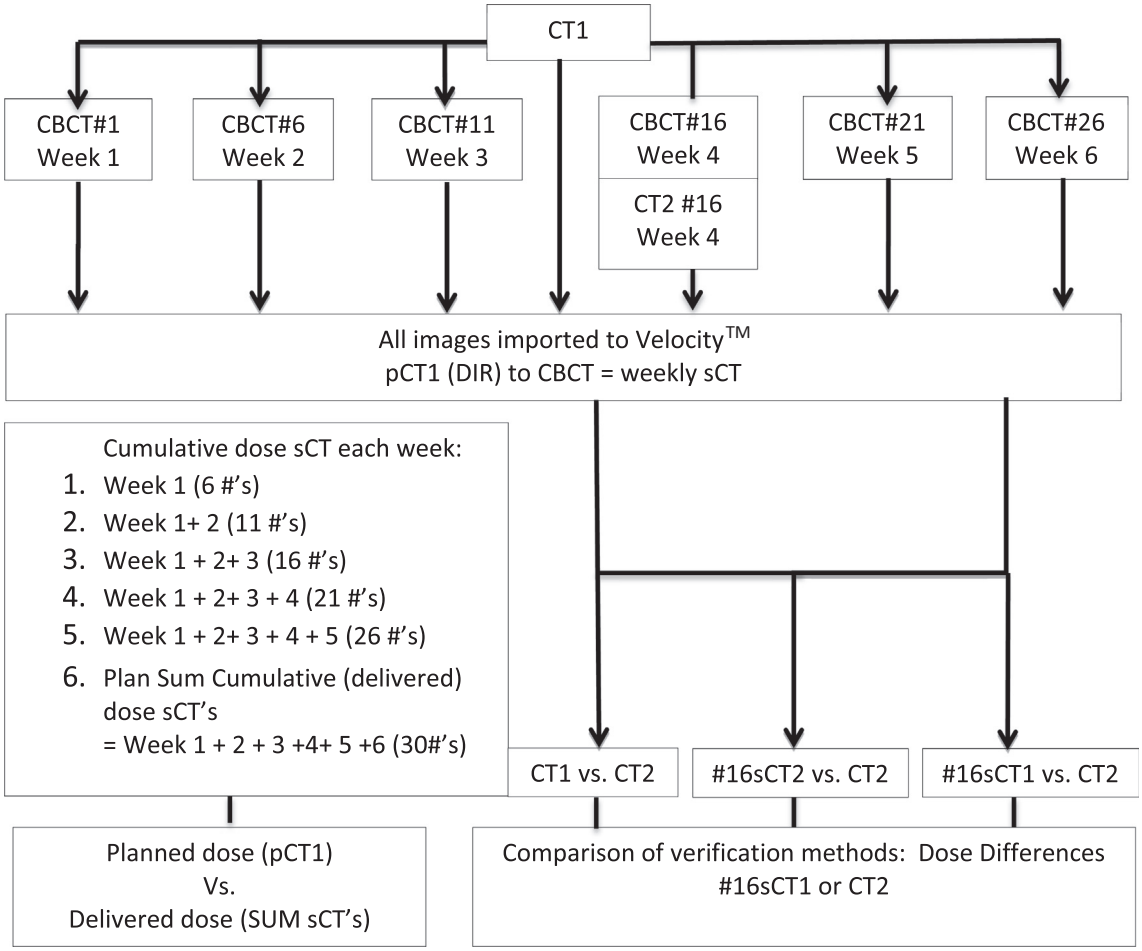

Fig. 2. Study flow.

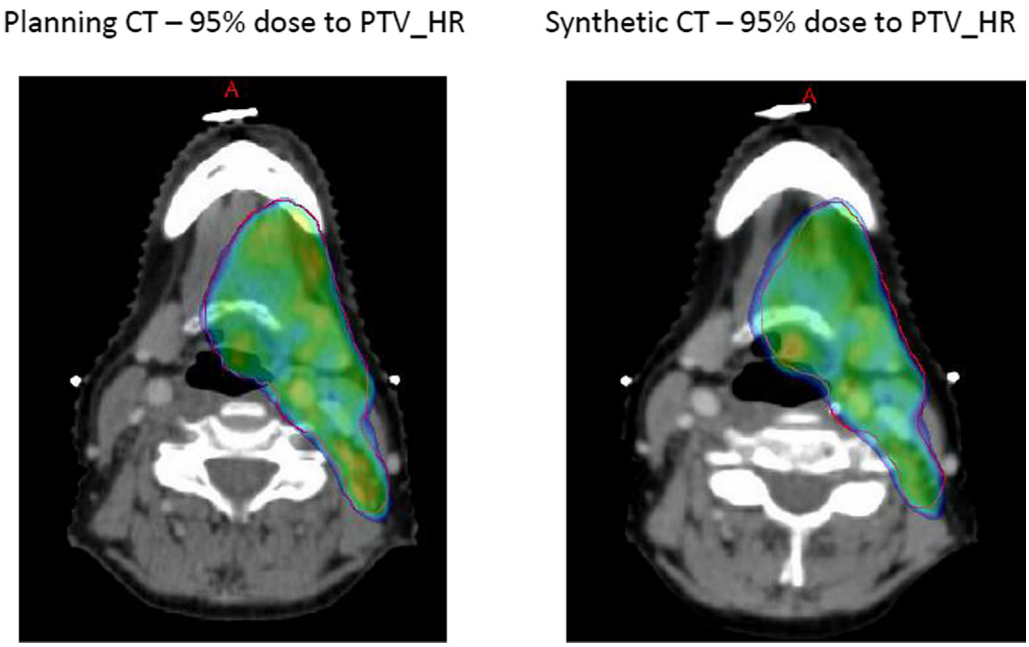

Fig. 3. Example of 95% dose distribution between the synthetic CT and planning CT1 at fraction 16.

re-calculated on pCT2, by applying the pre-set monitor unit values of the original pCT1 plan, allowing a visual evaluation of the treatment dose distribution on the repeat pCT2. The proximity of the dose to spinal cord and brainstem was given priority.

DIR between the fraction 16 CBCT and pCT2 was undertaken to create #16sCT2, as well as #16sCT1 (fraction 16 CBCT and pCT1). A rigid image registration between each fraction 16 CBCT and pCT2 was performed, within the selected ROI as previously described. The structure set from the fraction 16 CBCT with the parotid glands re-delineated was applied to pCT2. The rigid registration was imported to Velocity^{TM} for DIR to generate #16sCT2. A further rigid registration in the TPS to align the fraction 16 CBCT and #16sCT2 was performed and the structure set copied from CBCT to the #16sCT2. This allowed a QA evaluation of the #16sCT2 re-calculated dose, compared with the pCT2 dose calculation both undertaken at the same point in treatment. Identical image registration and dose assessment procedures were used as previously described.

Data collection

Planning and imaging information was collected from the department's TPS.

Patient information was stored and analysed anonymously.

Data analysis

Paired t-tests were used to analyse statistical differences in mean dose and volumes for plans based on the original pCT1 and sCTs at fractions 1, 6, 11, 16, 21 and 26. Repeated measures ANOVA were used to test for differences between weekly sCTs. The 'planned' cumulative dose based on the pCT1 was compared to the 'observed' cumulative dose based on the sum of the dose derived from the sCT plans. Bland-Altman limits of agreement were calculated at fraction 16 between #16sCT1 and CT2. All statistical tests were 2 sided and a significance level of 0.05 was applied.

Data analysis was carried out using Stata Statistical Software: Release 14 (TX: StataCorp LP).

Table 1
Tumour staging of patients.

T Stage:	%	n
0	5	1
1	25	5
2	31	6
3	25	5
4	14	3
N Stage:	%	n
1	65	13
2	30	6
3	5	1

Results

Patient demographics

20 consecutive patients were identified between October 2017 and January 2018. Sixty-five percent were male and 35% female, median age was 59 years (range 47–72). Sub-sites treated included tonsil (11), base of tongue (4), oropharynx not otherwise specified (4) and pharyngeal wall (1). 70% of patients had human papilloma virus (HPV) related SCCs and 80% received chemotherapy. TNM classification is shown in Table 1.

Image evaluation & anatomical changes

138 synthetic CT scans were evaluated, an example is shown in Fig. 3. The generated sCT image sets were found to be visually acceptable unless contour differences between the CBCT and pCT1 were greater than 1 cm (Fig. 4).

1 patient at fraction 16 had a gap on CBCT > 1 cm, which was not demonstrated on the sCT. This increased to 4, then 5 patients at fractions 21 and 26 respectively. Therefore 10 sCT scans generated during the DIR had the gap from the CBCT underestimated.

The gap between the immobilisation masks and the patient's body contour increased throughout treatment. By fraction 26 the CBCT mean gap was 0.92 cm (SD 0.45 cm) and 0.28 cm (SD 0.32 cm) based on the sCT (Table 2).

Both ipsilateral and contralateral PGs decreased in volume during treatment as shown in Table 3.

Comparison of weekly sCT single fraction dose

The mean single fraction dose to the ipsilateral parotids increased from 137.2 cGy at planning to 146.4 cGy at week 6 (dif-

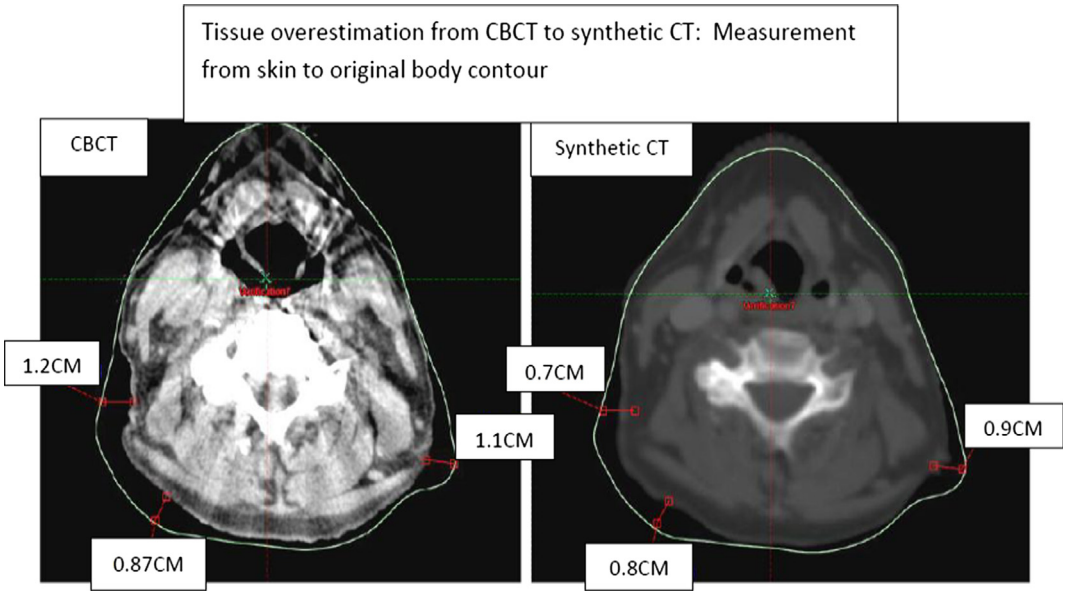

Fig. 4. Tissue overestimation on synthetic CT.

Table 2
Variation in gap at Isocentre between CBCT and synthetic CT at fractions 16, 21 & 26.

	Maximum Gap at Isocentre from skin surface to BDS					
	#16 (cm)		#21 (cm)		#26 (cm)	
	CBCT	sCT	CBCT	sCT	CBCT	sCT
Mean	0.53	0.25	0.84	0.35	0.92	0.28
SD	0.40	0.29	0.33	0.35	0.45	0.32
Median	0.65	0.20	0.80	0.30	0.75	0.20
Range	0–1.2	0–0.9	0–1.5	0–1	0–2	0–1

*Beam Direction Shell (BDS).

Table 3
Mean volume and dosimetry values at each week for one fraction.

		Mean (SD)														ANOVA* p value
		Planning CT		Week 1		Week 2		Week 3		Week 4		Week 5		Week 6		
Volume (CC)	Ipsilateral Parotid gland	28.8	(11.5)	29.0	(11.5)	28.3	(11.1)	27.4	(11.2)	26.1	(11.2)	24.1	(10.2)	22.7	(9.4)	<0.0001
	Contralateral Parotid gland	28.6	(10.6)	28.5	(11.0)	27.9	(9.8)	26.9	(9.8)	26.1	(9.9)	24.1	(9.0)	23.5	(9.4)	<0.0001
Mean Dose (cGy)	PTV_HR	218.2	(1.3)	218.1	(1.3)	217.7	(2.4)	217.8	(1.8)	218.1	(1.8)	218.2	(1.9)	217.9	(1.8)	0.42
	Ipsilateral parotid gland	137.2	(25.2)	137.6	(28.7)	136.7	(29.8)	136.6	(30.0)	136.8	(27.8)	142.2	(29.0)	146.4	(29.4)	<0.0001
	Contralateral parotid gland	86.9	(31.2)	89.4	(31.3)	88.1	(30.3)	89.0	(31.0)	89.7	(31.1)	92.0	(31.6)	93.3	(33.2)	0.0162
D95%	PTV_HR	96.6	(1.8)	95.5	(3.2)	95.2	(2.9)	94.8	(3.4)	95.1	(2.6)	94.4	(3.6)	94.6	(3.2)	0.34
Maximum dose (cGy)	PRV_Brainstem	146.2	(12.9)	145.4	(20.9)	146.2	(20.3)	147.1	(21.0)	146.9	(21.3)	146.4	(19.2)	150.8	(20.2)	0.39
	PRV_Spinal cord	139.5	(6.5)	140.7	(15.2)	141.0	(14.7)	143.4	(17.6)	142.5	(15.0)	142.8	(13.9)	142.3	(15.1)	0.87

*ANOVA test of difference between mean values across weeks.

ference 9.2 cGy 95%CI (4.4–14.0)), and the mean dose to the contralateral parotids rose from 86.9 cGy to 93.3 cGy (difference 6.4 cGy 95%CI (2.5–10.4)). The mean dose to PTV_HR did not vary (p = 0.42) during treatment, but D95% was smaller at week 6 (94.6%) compared to what had been planned (96.6%) (difference 2.0%, 95% CI (0.8–3.1), p = 0.0). Overall, there was no statistically significant difference in PRV_brainstem or PRV_spinal cord Dmax, however Dmax displayed greater variation than shown at planning.

Cumulative dose comparison

Table 4 shows the difference in 'observed' and 'planned' cumulative dose to organs. The difference in the observed and planned cumulative mean dose was −10 cGy (range −90 to 90 cGy) for PTV_HR, and 50 cGy (range −340 to 440 cGy) and 90 cGy (range −550 to 470 cGy) for the ipsilateral and contralateral parotids respectively. The mean difference in cumulative maximum dose to PRV_spinal cord and PRV_brainstem was 80 cGy (range −310 to 950 cGy) and 20 cGy (range −720 to 630 cGy) respectively.

Based on the sCTs one patient exceeded the PRV_spinal cord constraint Dmax < 4800 cGy - the dose was 5180 cGy. All patients were within the Dmax constraint for PRV_brainstem. The difference in the planned and observed relative dose received by 95% of the PTV_HR varied from −6.0% to 0.4% with a mean difference of −1.8% (95%CI −2.6 to −1.0%). Based on the pCT 19 of the 20 plans achieved the constraint D95%≥95 to PTV_HR throughout treatment but based on sCTs this was only 13 (65%).

Plan comparisons fraction 16

Table 5 shows the mean dose to the original structures based on the fraction 16 sCTs and pCT2 at week 4 are similar, between both verification modalities.

All 20 patients' met the dose constraints for Dmax to PRV_brainstem based on the #16sCT1 plans, however the PRV_spinal cord constraint failed in 3 patients. In contrast all patients passed the PRV_spinal cord constraint based on CT2.

Fig. 5 shows the Bland-Altman limits of agreement of dosimetry measures comparing #16sCT1 and CT2. Agreement between mean doses to PTV_HR was within approximately +/−3cGY. For mean dose to the ipsilateral and contralateral PG's the values lay within approximately +/− 20 cGy. For maximum dose to PRV_brainstem and PRV_spinal cord the limits of agreement suggest that #16sCT1

Table 4
Observed and planned cumulative dose based on planning CT and weekly synthetic CTs.

		Cumulative dose (cGy) or (%)				Difference (cGy) or (%)		
		Planned	Range	Observed	Range	mean difference	range	95% CI for mean difference
Mean dose	PTV_HR	6550	6480 to 6610	6540	6420 to 6610	−10	−90 to 90	−20 to 10
	Ipsilateral parotid gland	4120	3000 to 5940	4170	2780 to 5990	50	−340 to 440	−50 to 160
	Contralateral parotid gland	2610	440 to 3970	2700	430 to 3940	90	−550 to 470	−20 to 210
Max dose	PRV_Brainstem	4390	3350 to 4920	4410	3120 to 5350	20	−720 to 630	−130 to 170
	PRV_Spinal Cord	4180	3590 to 4460	4260	3330 to 5180	80	−310 to 950	−70 to 230
D95%	PTV_HR	96.6	90.2 to 98.4	94.8	86.6 to 97.9	−1.8	−6.0 to 0.4	−2.6 to −1.0

Table 5
Comparison of volumes and dosimetry based on a synthetic CT created from CT1 with CT2 at fraction 16.

		Planning CT1		#16 synthetic CT1		CT2 at fraction 16		#16 synthetic CT2	
		Mean	**SD**	**Mean**	**SD**	**Mean**	**SD**	**Mean**	**SD**
Volume (cc)	Ipsilateral Parotid Gland	28.8	(11.5)	26.1	(11.2)	26.1	(11.3)	26.3	(11.3)
	Contralateral Parotid Gland	28.6	(10.6)	26.1	(9.9)	25.9	(10.0)	26.2	(10.0)
Mean dose (cGy)	PTV_HR	218.2	(1.3)	218.1	(1.8)	218.4	(2.2)	218.1	(2.3)
	Ipsilateral	137.2	(25.2)	136.8	(27.8)	137.2	(27.6)	136.7	(27.0)
	contralateral	86.9	(31.2)	89.7	(31.1)	87.0	(29.9)	86.8	(29.2)
Maximum dose (cGy)	PRV_Brainstem	146.2	(12.9)	146.9	(21.3)	143.0	(17.0)	145.5	(23.7)
	PRV_Spinal Cord	139.5	(6.5)	142.5	(15.0)	138.3	(9.3)	140.9	(15.5)
D95%	PTV_HR	96.6	(1.8)	95.1	(2.6)	94.9	(4.5)	93.6	(6.9)
		n	**(%)**	**n**	**(%)**	**n**	**(%)**	**n**	**(%)**
D95%<95%	PTV_HR	1	(5)	6	(30)	6	(30)	7	(35)

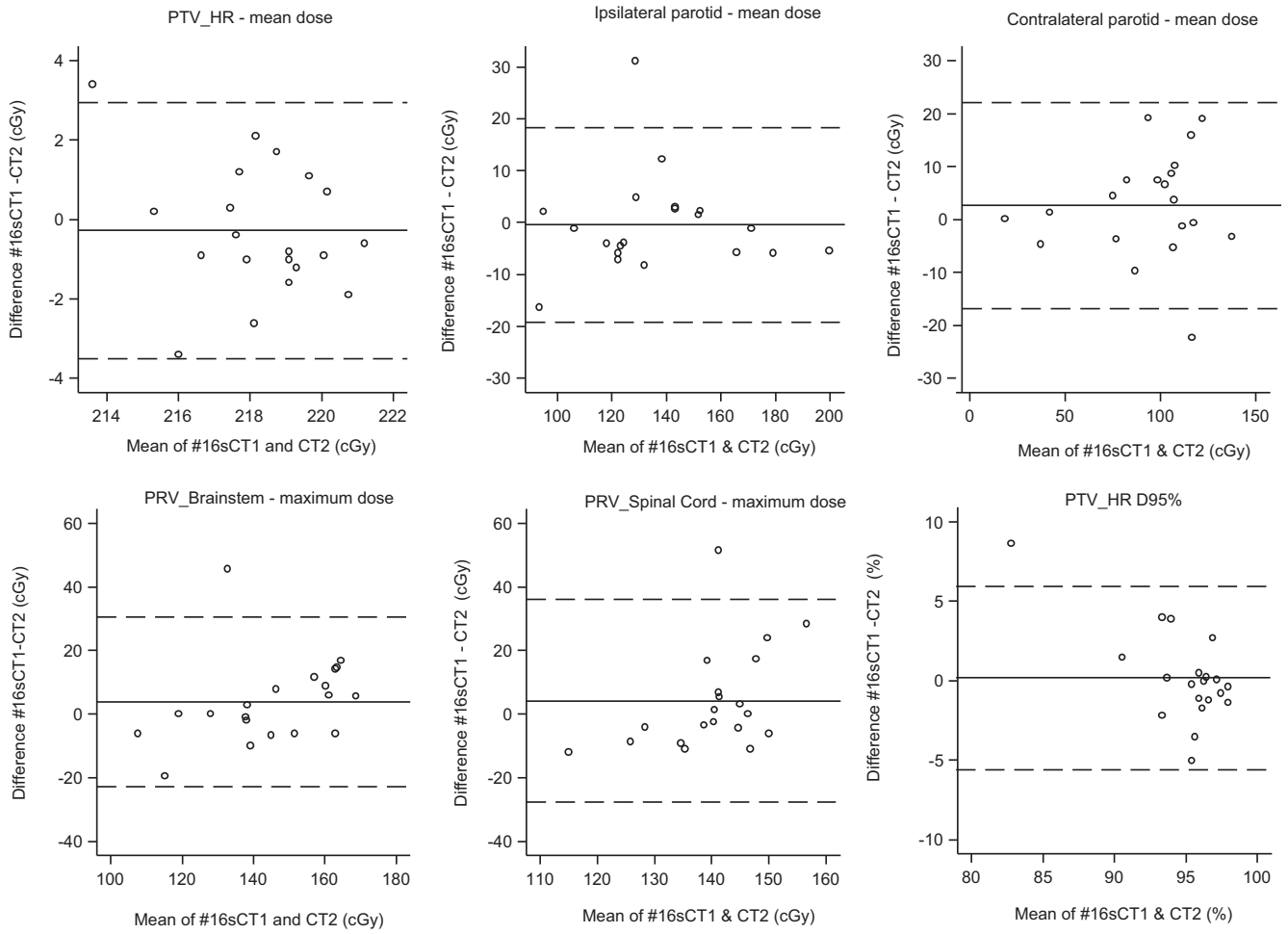

Fig. 5. Limits of agreement between #16sCT1 and CT2 mean dose differences.

underestimates the maximum dose when the dose is low and over estimates it when the dose is high, but overall the values were approximately within +/−30 cGy. PTV_HR is approximately within +/−5% but there is also a suggestion that PTV_HR D95% is over estimated when the dose is lower and under estimated when it is higher.

Discussion

This study explored the use of CBCT and synthetic CT to calculate dose and guide ART in H&N patients. The differences we found in the dosimetry data between the planning CT and synthetic CTs generated during treatment were small. Previous studies report uncertainty in the use of DIR as a clinical tool for verifying cumulative doses due to differences found between DIR algorithms [8,22–24].

Synthetic CT and anatomical change

The majority of the deformations generated sCT images without gross distortions when compared to the original CBCT, although distortion on some of the sCT images was observed. Anatomical changes can be well visualised on CBCT to evaluate changes in tar-

get volume, patient contour variation (caused by weight loss, tumour changes etc.) and shifts in delineated planning volumes [8,16,25,28]. One patient within this study had bolus in situ during their CBCT scans but not on their pCT. This created extra tissue on the generated sCT. The bolus was not included in the delineated body outline; therefore it had no effect on the dose calculations within the TPS. The patient's, CBCT displayed regression of a nodal GTV at week 6 measuring 1.5 cm. This did not trigger replanning, as the residual disease volume was still well contained within the PTV and the dose coverage remained adequate. This study visually assessed delineated structures and patient contour changes. Other anatomical variations will be assessed in future work. A recent study evaluated contour changes > 1.5 cm between generated sCTs and CBCT to guide ART during treatment [26]. Our study identified that when patient's contour changes were > 1 cm the DIR software failed to correctly recognise the soft tissue during the deformation, although this had a minimal effect on the calculated dose distributions. Previous studies confirm this finding, reporting that image quality with DIR deteriorates during the treatment course, as the algorithm struggles to account for large changes in volumes [22–27]. In such cases where deformation is still unacceptable after corrections applied, repeat CT would be necessary to make accurate clinical decisions and volume amendments.

Dose comparison between sCT and pCT

Defining spinal cord and brainstem tissue on CBCT is challenging due to poor image contrast [27]. Consequently we did not revolume these structures. A limitation of this study is that the structure set was not deformed and DVH statistics are based on the original structures, except the parotid glands. To ensure the other structures were still valid, a visual check of the structures applied to the sCT was carried out. Future work will investigate structure deformation as it is recognised this may provide better representation of the dose to the structures based on that fraction's anatomical positioning. Acquiring extended CBCT scans, or prioritising the acquisition of structures contained within the FOV, could allow these volumes to be assessed in more detail [4,24]. This is an area of work being investigated currently.

We did identify a reduction in parotid gland volumes during treatment based on the CBCT delineations and the synthetic CT dose calculations showed an increasing mean dose to the parotids at each fraction they were generated. Dose delivered to the gross disease is given priority therefore any dose increase to the ipsilateral parotid gland would not trigger re-planning due to the close proximity of the PTV_HR. Adaptive planning to spare the contralateral PG is not standard practice in our Centre, although other studies have reported this [28].

For PTV_HR no difference between the planned and observed mean dose was detected, although D95% was lower at week 6 by 2% on the sCT plans. This observed reduction in the dose to 95% of PTV_HR may be a result of the short CBCT FOV, as the entire PTV_HR structure was not consistently captured within the scan extent. Further assessment of the structures within the FOV is necessary to determine this. We also detected a cumulative decrease of −1.8% in the 95% dose delivered to PTV_HR between the planned and observed doses. The reduction in dose to the target volume is consistent with findings in other studies [29,30].

Verification at mid-treatment sCT vs. pCT2

At fraction 16 the differences in the synthetic CT plans created by deforming the CBCT with both CT1 and CT2 were compared. We found no statistically significant differences between the plan calculations based on #16sCT1 and pCT2. This suggests that dose constraint evaluation on the #16sCT1 might be a useful planning guide. Dose constraints were achieved for all patients at fraction 16 using the repeat pCT2 verification plan; however 3 patients failed the PRV_spinal cord constraint on the #16sCT1 plan. Evaluation of the difference in the mean maximum doses between #16sCT1 and pCT2 using Bland Altman limits of agreement suggested potential proportional biases in the sCT calculated doses to PRV_spinal cord and PRV_brainstem. The Bland Altman plots suggested that #16sCT1 underestimated Dmax when the dose is low and overestimated Dmax when the dose is high. The net effect is that calculations based on sCT would potentially trigger more re-plans than necessary, which is in agreement with previous study findings [14]. This cautious process would not compromise patient safety. The mean dose to PTV_HR between CT1 and CT2 remained the same at fraction 16, although D95% declined. This requires further assessment of the dose coverage to PTV_HR during treatment to ensure the delivered dose does not become unacceptable, potentially increasing patient's risk of recurrence. Further investigation of this finding is necessary as dose to PTV_HR is not formally reassessed at fraction 16 within our current protocol. DVH statistics were also comparable at fraction 16, though awareness of the limitations of DIR is essential when assessing volumes.

Anatomical changes are reported to occur early within the first 4 weeks of RT, justifying the need for repeated imaging and replanning during this period [8,14,15,25,28]. A verification process such as described here would increase availability on CT for all treatment sites within this busy department, whilst potentially reducing patient anxiety as many expect 'results' from the repeat planning CT. The safe omission of repeat CT during H&N RT has been previously justified [4,31]. Many institutions already acknowledge the benefit of rigid registrations using CBCT for on-treatment image guidance; and identifying anatomical changes. However, the widespread implementation of CBCT used for DIR as a sole dose verification modality in the clinical setting is constrained by its limitations and complexity. In particular, DIR remains problematic in cases where large changes in patient contour are identified [1,4,13].

Conclusions

Synthetic CT verification provides similar dose calculations to those of a repeat planning CT. There are limitations and uncertainties in the use of DIR and its algorithms which must be fully understood before such a process is applied routinely in the clinical setting. When this is achieved, sCT could stratify patients requiring planning interventions, at more targeted time points during the treatment course. If replanning was considered necessary on the basis of sCT dosimetry, patients could then undergo a repeat planning CT for confirmation, with adaptive planning being performed on the pCT. This would eliminate routine repeat pCTs for dose verification, thereby leading to a reduction in the number of pCTs required, with the necessary scans obtained at the most appropriate time point.

Advances in knowledge

This study presents an evaluation of head and neck dose verification during radiotherapy with the objective of reducing routine repeat CT scans, demonstrating the potential of CBCT and synthetic CT as a feasible approach for verification, whilst describing the limitations of this methodology.

Declaration of Competing Interest

The authors declare that they have no known competing financial interests or personal relationships that could have appeared to influence the work reported in this paper.

Acknowledgement

Thank you to the Beatson Cancer Charity.

References

[1] Elstrøm UV, Wysocka BA, Muren LP, Petersen JBB, Grau C. Daily kV cone-beam CT and deformable image registration as a method for studying dosimetric consequences of anatomic changes in adaptive IMRT of head and neck cancer. Acta Oncol 2010;49(7):1101–8. https://doi.org/10.3109/0284186X.2010.500304.

[2] Mortensen HR, Overgaard J, Specht L, Overgaard M, Johansen J, Evensen JF, et al. Prevalence and peak incidence of acute and late normal tissue morbidity in the DAHANCA 6&7 randomised trial with accelerated radiotherapy for head and neck cancer. Radiother Oncol 2012;103(1):69–75. https://doi.org/10.1016/j.radonc.2012.01.002.

[3] Hermans BC, Persoon LC, Podesta M, Hoebers FJ, Verhaegen F, Troost EG. Weekly kilovoltage cone-beam computed tomography for detection of dose discrepancies during (chemo) radiotherapy for head and neck cancer. Acta Oncol 2015;54(9):1483–9. https://doi.org/10.3109/0284186X.2015.1061210.

[4] Ayyalusamy A, Vellaiyan S, Shanmugam S, Ilamurugu A, Gandhi A, Shanmugam T, et al. Feasibility of offline head & neck adaptive radiotherapy using deformed planning CT electron density mapping on weekly cone beam computed tomography. Br J Radiol 2017;90(1069):20160420. https://doi.org/10.1259/bjr.20160420.

[5] Hansen CR, Bertelsen A, Hazell I, Zukauskaite R, Gyldenkerne N, Johansen J, et al. Automatic treatment planning improves the clinical quality of head and neck cancer treatment plans. Clin Translational Radiat Oncol 2016 December;2016(1):2–8. https://doi.org/10.1016/j.ctro.2016.08.001.

[6] Rigaud B, Simon A, Castelli J, Gobeli M, Ospina Arango JD, Cazoulat G, et al. PO-0935: Evaluation of deformable image registration methods for dose monitoring in head and neck adaptive radiotherapy. Radiother Oncol 2015 April;2015(115):S488–9. https://doi.org/10.1155/2015/726268.

[7] Müller BS, Duma MN, Kampfer S, Nill S, Oelfke U, Geinitz H, et al. Impact of interfractional changes in head and neck cancer patients on the delivered dose in intensity modulated radiotherapy with protons and photons. Physica Med 2015;31(3):266–72. https://doi.org/10.1016/j.ejmp.2015.02.007.

[8] van Kranen S, Hamming-Vrieze O, Wolf A, Damen E, van Herk M, Sonke J. Head and neck margin reduction with adaptive radiation therapy: robustness of treatment plans against anatomy changes. Int J Radiat Oncol Biol Phys 2016;96(3):653–60. https://doi.org/10.1016/j.ijrobp.2016.07.011. 1 November 2016.

[9] Houweling AC, van der Meer S, van der Wal E, Terhaard CHJ, Raaijmakers CPJ. Improved immobilization using an individual head support in head and neck cancer patients. Radiotherapy Oncology 2010 July 2010;96(1):100–103. https://doi.org/10.1016/j.radonc.2010.04.014.

[10] Hvid CA, Elstrøm UV, Jensen K, Alber M, Grau C. Accuracy of software-assisted contour propagation from planning CT to cone beam CT in head and neck radiotherapy. Acta Oncol 2016;55(11):1324–30. https://doi.org/10.1080/0284186X.2016.1185149.

[11] Bell K, Licht N, Rübe C, Dzierma Y. Image guidance and positioning accuracy in clinical practice: influence of positioning errors and imaging dose on the real dose distribution for head and neck cancer treatment. Radiat Oncol 2018;13:190. https://doi.org/10.1186/s13014-018-1141-8.

[12] Kumarasiri K, Siddiqui F, Liu C, Yechieli R, Shah M, Pradhan D, et al. Deformable image registration based automatic CT-to-CT contour propagation for head and neck adaptive radiotherapy in the routine clinical setting. Int J Med Phys 2014;41(12). https://doi.org/10.1118/1.4901409. pp. 121712–1- 121712–10.

[13] Leech M, Coffey M, Mast M, Moura F, Osztavics A, Pasini D, et al. Guidelines for positioning, immobilisation and position verification of head and neck patients for RTTs. ESTRO 2016. https://doi.org/10.1016/j.tipsro.2016.12.001.

[14] Bhandari V, Patel P, Gurjar OP, Gupta KL. Impact of repeat computerized tomography replans in the radiation therapy of head and neck cancers. J Med Phys 2014 Jul;39(3):164–8. http://www.jmp.org.in/text.asp?2014/39/3/164/139005.

[15] Brown E, Owen R, Harden F, Mengersen K, Oestreich K, Houghton W, et al. Predicting the need for adaptive radiotherapy in head and neck cancer. Radiotherapy Oncol 2015 July 2015; 116(1):57–63. http://dx.doi.org/10.1016/j.radonc.2015.06.02.

[16] Noble DJ, Yeap P, Seah SYK, Harrison K, Shelley LEA, Romanchikova M, et al. Anatomical change during radiotherapy for head and neck cancer, and its effect on delivered dose to the spinal cord. Radiother Oncol 2019 January;2019(130):32–8. https://doi.org/10.1016/j.radonc.2018.07.009.

[17] Chuter R, Prestwich R, Bird D, Scarsbrook A, Sykes J, Wilson D, et al. The use of deformable image registration to integrate diagnostic MRI into the radiotherapy planning pathway for head and neck cancer. Radiotherapy Oncol 2017 February 2017;122(2):229-235. https://doi.org/10.1016/j.radonc.2016.07.016.

[18] Grégoire V, Grau C, Lapeyre M, Maingon P. Target volume selection and delineation (T and N) for primary radiation treatment of oral cavity, oropharyngeal, hypopharyngeal and laryngeal squamous cell carcinoma. Oral Oncol 2018 December;2018(87):131–7. https://doi.org/10.1016/j.oraloncology.2018.10.034.

[19] Grégoire V, Ang K, Budach W, Grau C, Hamoir M, Langendijk JA, et al. Delineation of the neck node levels for head and neck tumors: A 2013 update. DAHANCA, EORTC, HKNPCSG, NCIC CTG, NCRI, RTOG, TROG consensus guidelines. Radiotherapy Oncol 2014;110:172–81. https://doi.org/10.1016/j.radonc.2013.10.010.

[20] Nutting CM, Morden JP, Harrington KJ, Urbano TG, Bhide SA, Clark C, et al. Parotid-sparing intensity modulated versus conventional radiotherapy in head and neck cancer (PARSPORT): a phase 3 multicentre randomised controlled trial. Lancet Oncol 2011;12(2):127–36. https://doi.org/10.1016/S1470-2045(10)70290-4.

[21] Varian medical systems, Velocity user manual. Velocity 3.2.0. Published USA; 2016. Available from: https://www.varian.com/sites/default/files/resource_attachments/Velocity3.2.0DicomConformanceStatement.pdf.

[22] Veiga C, Lourenço AM, Mouinuddin S, van Herk M, Modat M, Ourselin S, et al. Toward adaptive radiotherapy for head and neck patients: Uncertainties in dose warping due to the choice of deformable registration algorithm. Med Phys 2015;42(2):760–9. https://doi.org/10.1118/1.4905050.

[23] Eiland RB, Maare C, Sjostrom D, Samsoe E, Behrens CF. Dosimetric and geometric evaluation of the use of deformable image registration in adaptive intensity-modulated radiotherapy for head-and-neck cancer. J Radiat Res 2014;55(5):1002–8. https://doi.org/10.1016/S0167-8140(12)71226-4.

[24] Mencarelli A, van Kranen SR, Hamming-Vrieze O, van Beek S, Nico Rasch CR, van Herk M, et al. Deformable image registration for adaptive radiation therapy of head and neck cancer: accuracy and precision in the presence of tumor changes. Int J Radiat Oncol Biol Phys 2014;90(3):680–7. https://doi.org/10.1016/j.ijrobp.2014.06.045.

[25] van Beek S, Jonker M, Hamming-Vrieze O, Al-Mamgani A, Navran A, Remeijer P, et al. Protocolised way to cope with anatomical changes in head & neck cancer during the course of radiotherapy. Tech Innovations Patient Support Radiat Oncol 2019;12:34–40. https://doi.org/10.1016/j.tipsro.2019.11.001.

[26] Weppler S, Quon H, Banerjee R, Schinkel C, Smith W. Framework for the quantitative assessment of adaptive radiation therapy protocols. J Appl Clin Med Phys 2018;19(6):26–34. https://doi.org/10.1002/acm2.12437.

[27] Roussakis YG, Dehghani H, Green S, Webster GJ. Validation of a dose warping algorithm using clinically realistic scenarios. Br J Radiol 2015 May;88:1049. https://doi.org/10.1259/bjr.20140691.

[28] Brouwer CL, Steenbakkers RJHM, Langendijk JA, Sijtsema NM. Identifying patients who may benefit from adaptive radiotherapy: Does the literature on anatomic and dosimetric changes in head and neck organs at risk during radiotherapy provide information to help? Radiother Oncol 2015;115(3):285–94. https://doi.org/10.1016/j.radonc.2015.05.018. June 2015.

[29] Surucu M, Shah KK, Roeske JC, Choi M, Small W, Emami B. Adaptive radiotherapy for head and neck cancer: implications for clinical and dosimetry outcomes. Technol Cancer Res Treat 2017;16(2):218–23. https://doi.org/10.1177/1533034616662165.

[30] Grégoire V, Jeraj R, Lee JA, O'Sullivan B. Radiotherapy for head and neck tumours in 2012 and beyond: conformal, tailored, and adaptive? Lancet Oncol 2012;13(7):e292–300. https://doi.org/10.1016/S1470-2045(12)70237-1. July 2012.

[31] Hvid CA, Elstrøm UV, Jensen K, Grau C. Cone-beam computed tomography (CBCT) for adaptive image guided head and neck radiation therapy. Acta Oncol 2018;57(4):552–6. https://doi.org/10.1080/0284186X.2017.1398414.